Merging of unequal mass binary black holes in non-axisymmetric galactic nuclei

Peter Berczik[1,2,3] , Manuel Arca Sedda[4] , Margaryta Sobolenko[3] , Marina Ishchenko[3] , Olexander Sobodar[3] ,
and Rainer Spurzem[1,5]

[1] Astronomisches Rechen-Institut, Zentrum für Astronomie, University of Heidelberg, Mönchhofstrasse 12-14, 69120, Heidelberg, Germany
[2] Konkoly Observatory, Research Centre for Astronomy and Earth Sciences, Eötvös Loránd Research Network (ELKH), MTA Centre of Excellence, Konkoly Thege Miklós út 15-17, 1121 Budapest, Hungary
[3] Main Astronomical Observatory, National Academy of Sciences of Ukraine, 27 Akademika Zabolotnoho St., 03143 Kyiv, Ukraine
e-mail: berczik@mao.kiev.ua
[4] Physics and Astronomy Department Galileo Galilei, University of Padova, Vicolo dell'Osservatorio 3, I–35122, Padova, Italy
[5] Kavli Institute for Astronomy and Astrophysics, Peking University, Yiheyuan Lu 5, Haidian Qu, 100871, Beijing, China

ABSTRACT

In this work, we study the stellar-dynamical hardening of unequal mass supermassive black hole (SMBH) binaries in the central regions of merging galactic nuclei. We present a comprehensive set of direct N-body simulations of the problem, varying both the total mass and the mass ratio of the SMBH binary (SMBHB). Simulations were carried out with the $\varphi-$GPU N-body code, which enabled us to fully exploit supercomputers equipped with graphic processing units (GPUs). As a model for the galactic nuclei, we adopted initial axisymmetric, rotating models, aimed at reproducing the properties of a galactic nucleus emerging from a galaxy merger event, containing two SMBHs which were unbound initially. We found no 'final-parsec problem', as our SMBHs tend to pair and shrink without showing significant signs of stalling. This confirms earlier results and extends them to large particle numbers and rotating systems. We find that the SMBHB hardening depends on the binary-reduced mass ratio via a single parameter function. Our results suggest that, at a fixed value for the SMBHB primary mass, the merger time of highly asymmetric binaries is up to four order of magnitudes smaller than the equal-mass binaries. This can significantly affect the population of SMBHs potentially detectable as gravitational wave sources.

Key words. black holes – binary black holes — galactic nuclei – stellar dynamics

1. Introduction

According to the hierarchical structure formation scenario in the Λ cold dark matter (ΛCDM) paradigm, bright massive galaxies are supposed to form through mergers and the accretion of smaller galaxies. Supermassive black holes (SMBHs) are commonly observed at the centres of most galaxies, and their mass correlates to several properties of their host galaxy, such as bulge mass (Ho & Kim 2014) or central velocity dispersion (see e.g. Gültekin et al. 2009). Therefore, if the majority of galaxies harbour an SMBH in their centres, SMBH binaries (SMBHBs) should represent an unavoidable outcome of the hierarchical formation scenario (Begelman et al. 1980).

Several examples of resolved SMBHBs with a separation of less than 1 kpc are known. The tightest resolved binary is settled in galaxy 0402+379 and was identified via radio observations achieved with the Very Long Baseline Interferometer (VLBI; Rodriguez et al. 2006; Bansal et al. 2017). It contains an SMBH pair candidate with a total mass $\sim 10^8$ M$_\odot$ and a separation of 7.3 pc. The most reliable and intensively observed SMBHB candidate was placed in a nearby ultraluminous infrared galaxy NGC 6240 (Komossa et al. 2003). Two components (South and North) were resolved in X-ray at a separation of 750 pc. High-resolved observations with the MUSE instrument revealed the possibility of the third smallest component

presence at south nuclei (Kollatschny et al. 2020; for the discussion, see Fabbiano et al. 2020). Using the $M_{\rm BH} - \sigma$ relation, BHs with masses of $3.6 \pm 0.8 \times 10^8$ M$_\odot$, $7.1 \pm 0.8 \times 10^8$ M$_\odot$, and $9.0 \pm 0.7 \times 10^7$ M$_\odot$ were obtained for North, South 1, and South 2 components, respectively. The recent optically and spectroscopically resolved binary in galaxy NGC 7727 has a separation of 500 pc and BH masses of $1.54^{+0.18}_{-0.15} \times 10^8$ M$_\odot$ and $6.33^{+3.32}_{-1.40} \times 10^6$ M$_\odot$ (Voggel et al. 2022). The OJ287 is an SMBHB candidate detected via quasi-periodic outbursts for which it has been possible to model the binary separation (~ 0.05 pc), eccentricity (~ 0.6), and spin (modelled taking even the spin-orbit interaction into account, see Valtonen 2007; Valtonen et al. 2010a,b).

The relativistic in-spiral and final coalescence are driven by gravitational wave (GW) emission, making SMBHBs among the strongest sources to be measured with future GW space satellite missions, such as the Laser Interferometer Space Antenna (LISA; Gong et al. 2011; Amaro-Seoane et al. 2013, 2017), or the TianQin (Luo et al. 2016), Taiji (Ruan et al. 2020), or μAres (Sesana et al. 2019) space detectors. It is therefore of paramount importance to understand the astrophysical processes that drive SMBHBs from the unbound, pre-merger state, into the relativistic regime and their associated efficiency. This information can be used to place robust, and physically motivated, constraints on the merger rate of these GW sources and provide a test bed for GW signal templates to be compared with future observations.

However, the large number of existing works focussed on full numerical simulations of SMBHs pairing and evolution have not fully covered all the important parameters' space yet. In particular, within the hierarchical galaxy formation scenario, the range of mass ratios in galaxy mergers can hugely vary from 1:1 (major mergers) to 1:3, down to minor mergers, that is with mass ratios even below 1:10 (cf. e.g. Naab et al. 2006, 2009). Given the correlations between galaxies and SMBHs masses, it is thus expected that also SMBHBs should form with a wide range of mass ratios. However, the majority of numerical studies based on *N*-body models have mostly focussed on nearly equal mass binaries. Moreover, the galactic nucleus produced in a galaxy merger event is expected to preserve a non-negligible rotation due to the global angular momentum conservation. The collective motion of stars affected by the rotation of the galactic nucleus can have a non-trivial effect on the SMBHB evolution. In this paper, we expand the simulations presented in Berczik et al. (2006) and Wang et al. (2014) by exploring a wider range of mass ratios, $0.01 - 1$, and by also taking the rotating nuclei into account.

Furthermore, the new simulations are based on our improved φ−GPU *N*-body code (Berczik et al. 2013b; Sobolenko et al. 2021), which implements general relativity effects in the form of post-Newtonian corrections to the equations of motion (Sobolenko et al. 2017; Khan et al. 2016). This will enable us to follow the SMBH binary evolution as a result of the simultaneous action of stellar hardening and GW emission all the way to final coalescence and allow us to model the GW signal during the final inspiral (Khan et al. 2013; Sobolenko et al. 2017; Khan et al. 2018).

The paper is structured as follows. In Section 2 we describe the initial conditions adopted in our *N*-body simulations; in Section 3 we describe how the modelled SMBHB hardening rate varies across the parameter space explored; and in Section 4 we summarize and discuss the main conclusions of our paper.

2. Units and initial conditions

We analysed a suite of 68 *N*-body simulations comprised of N = 25k, 50k, 100k, 200k, 400k, 1M particles, modelling the evolution of an SMBHB embedded in a rotating galactic nucleus, so as to reproduce the typical environment of the inner regions of a post-merged galaxy. Details about these simulations are provided in Berczik et al. (2006), Berentzen et al. (2009), and Wang et al. (2014). In this work, we focus on the shrinking of the SMBHB as it interacts with surrounding stars. Because the small *N* runs (namely 25k and 50k) have a larger uncertainty in the hardening results, we exclude them from the discussion of the further results. We can briefly summarize the main features of our models as follows.

The simulations presented in this work have been carried out using the direct *N*-body φ−GPU code. Our *N*-body package uses a high order Hermite integration scheme and individual block time steps (the code supports time integration of particle orbits with fourth, sixth, and even eighth order schemes). We refer the more interested readers to a general discussion about different *N*-body codes and their implementation in Berczik et al. (2011, 2013a). The φ−GPU code is fully parallelized using the MPI library. This code has been newly rewritten in C++ and based on the earlier CPU serial *N*-body code (YEBISU; Nitadori & Makino 2008). The MPI parallelization was done in the same '*j*' particle parallelization mode as in the earlier φ−GRAPE code (Harfst et al. 2007).
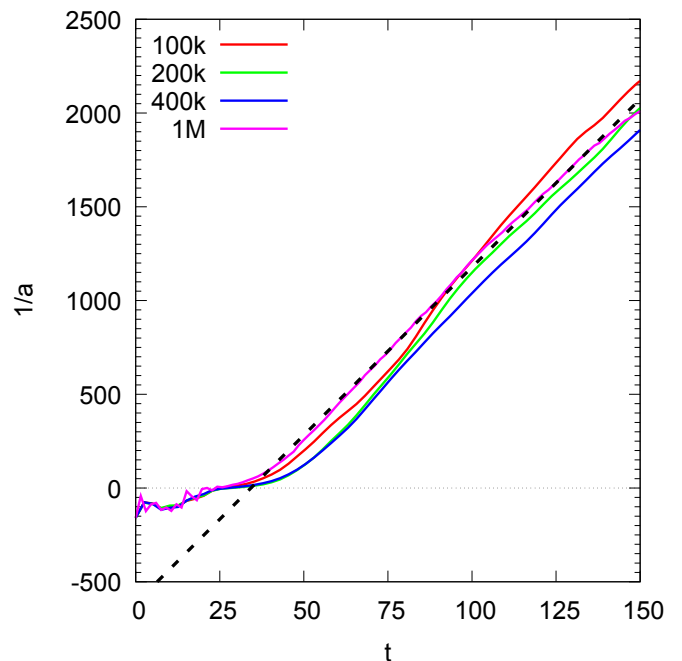
Fig. 1. Inverse of the binary's semi-major axis *a* as a function of time for the four different particles' numbers N = 100k, 200k, 400k, 1M model with an SMBH mass ratio of m_1:m_2=0.01:0.002. The black dashed line shows the common corresponding linear fit between the time interval $t = 50 - 150$.

The current version of the φ−GPU [1] code uses native GPU support and direct code access to the GPU using the NVIDIA native CUDA library. The code is designed to use different softening parameters for the gravity calculation (if it is required) for different astrophysical components in our simulations, such as SMBHs, dark matter, or stars particles. More details about the public version of the φ−GPU code and its performance are presented in Berczik et al. (2011, 2013a). The present code has been thoroughly tested and has already been used to obtain important results in our earlier large-scale (up to a few million body) simulations (Khan et al. 2018; Zhong et al. 2014; Li et al. 2012; Just et al. 2012).

All simulations are initially scaled by applying the standard strategy for *N*-body normalization [2] (Aarseth et al. 1974), according to which both the gravitational constant and the total mass of the stellar systems are set to unity, $G = M = 1$, and the total energy of the system is set to $E = -1/4$. The galactic nucleus initially follows a rotating King distribution function (see, e.g. Einsel & Spurzem 1999, and references therein). We set the dimensionless potential well (King parameter) and rotation parameters to $W_0 = 6$ and $\omega_0 = 1.8$, respectively, in all of our models. At the centre of the nucleus, we placed two SMBHs initially unbound with a primary mass $m_1 = (1-4) \times 10^{-2}$ times the nucleus mass and the mass ratio $q = 10^{-4} - 1$. The corresponding range of reduced mass adopted is thus $\mu \equiv m_1 m_2 / (m_1 + m_2) = 9.9 \times 10^{-3} - 2$. The total angular momentum vector of both the stellar nucleus and the SMBHs are aligned with the *z* axis of our coordinate frame. We placed the two SMBHs in the $z = 0$ mid-plane with initial coordinate components $x_{1,2} = 0$ and $y_{1,2} = \pm 0.3$, where the subscripts denote the two SMBHs.
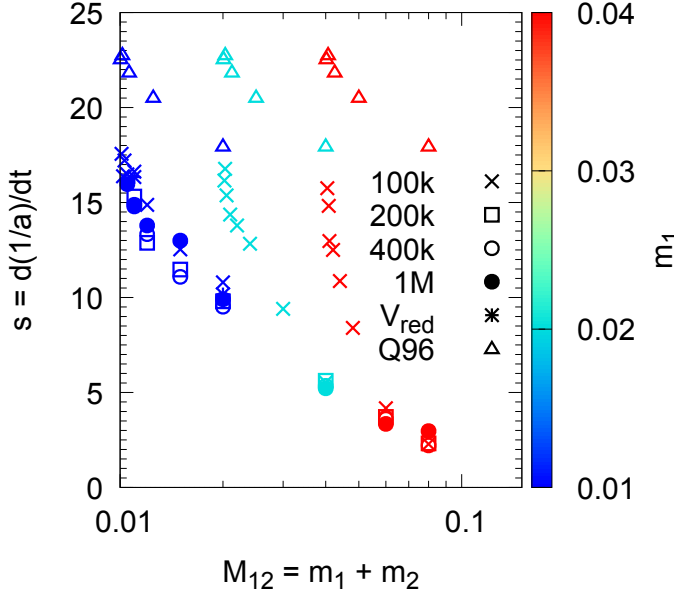
Fig. 2. Hardening rate for SMBH binaries with different mass ratios $q = m_2/m_1$ (it is important to note $m_1 \geq m_2$) as a function of the binaries' total mass $M_{12} = m_1 + m_2$. Different symbols represent models with different particle numbers N (see Table 1), respectively. The open triangle is a parameter H_0 (see Table 1 in Quinlan 1996). The colours are used to indicate the primary SMBH mass m_1.

It is important to note that the coordinates of SMBHs are given in N-body units and the distance from the centre of the SMBHs' particles roughly corresponds to the influence radius of models in which the SMBHB has a total mass of 2×10^{-2}. In all the
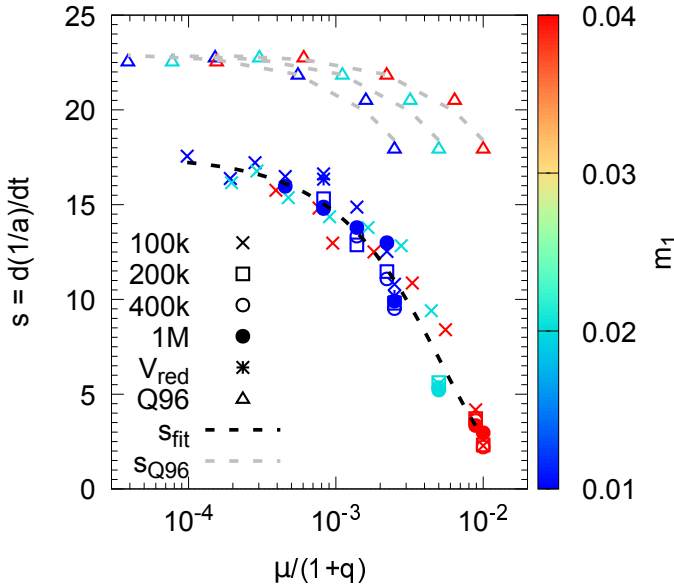

Fig. 3. Hardening rate as a function of the ratio between the reduced mass and the mass ratio, $\mu/(1 + q)$. Colour coding marks the mass of the primary component, whereas different symbols refer to different N models. The open triangle is a parameter H_0 (see Table 1 in Quinlan 1996). The hardening rate was fitted by equation 2.

tables and figures, we use these normalized N-body units (if not specified directly).

The initial velocities for the two SMBHs are oriented along the x axis and set to $v_{x;1,2} = \pm V_{\text{circ}}$, where V_{circ} is the circular velocity within the stellar background model of nuclei. We note that our choice of initial parameters and scaling implies a circular velocity $V_{\text{circ}} \approx 0.7$ in N-body units at the initial SMBH positions.

We complement our database of simulations with an extra set of four further models in which we assume for the SMBH the initial velocity $v_{x;1,2} = V_{\text{red}} = \pm 0.1 V_{\text{circ}} \approx 0.07$. This choice implies that the SMBHs initially move on more eccentric orbits compared to the other simulations, thus allowing them to pair in a shorter timescale. All the main features of our models are summarized in Table 1.

3. Results and discussion

Due to the initial rotation, the stellar distribution undergoes a strong initial bar instability and later forms a rotating triaxial nucleus, as has been discussed in our previous works (Berczik et al. 2006; Berentzen et al. 2009; Wang et al. 2014). The two SMBHs migrate inwards due to the dynamical friction until the point at which they become gravitationally bound.

After the SMBHB formation, continuous interactions with the surrounding field stars cause the shrinking of the orbit, that is to say there is a progressive decrease in the binary semi-major axis a. The semi-major axis evolution can be divided into two phases: one during which the binary orbit evolution is driven by both dynamical friction and stellar hardening and, another, dominated by stellar encounters during which the binary shrinking proceeds at a nearly constant rate. This process in basic steps was described and studied in previous classical works (Mikkola & Valtonen 1992; Makino & Funato 2004). The work of the highly eccentric SMBHB dynamical evolution in the environment of 'field stars' presented and described in Iwasawa et al. (2011) was especially important; it was shown that the eccentricity increase in SMBH binaries is driven by a combination of a secular effect impinged by the overall nucleus tidal field and a cumulative effect coming from the star-SMBHB scattering in a prograde configuration. In our simulations, these two effects are likely mixed, thus making it hard to discern between them. We postpone any analysis on the binary eccentricity evolution to a forthcoming paper, and we point the interested reader to our previous works for Newtonian simulations (Berentzen et al. 2009).

3.1. Hardening rate

Figure 1 shows the time evolution of the inverse of the binary semi-major axis ($1/a$) in the case of a set of models characterized by $m_1{:}m_2{=}0.01{:}0.002$, assuming $N = 100k$, $200k$, $400k$, and $1M$. The plot outlines that the hardening follows a nearly linear trend, regardless of the number of particles. Therefore the slope of the $1/a$ curve provides us with an estimate of the binary hardening rate, $s(t) = d(1/a)/dt$. The black dashed line in Figure 1 represents the best-fitting linear relation calculated for the time interval $t = 50-150$ (N-body units). Coupling the hardening rate with the extra hardening triggered by GW emission enables us to infer the binary merger time (e.g. Gualandris & Merritt 2012; Arca-Sedda & Gualandris 2018; Gualandris et al. 2022).

Figure 2 shows the dimensionless hardening rate for SMB-HBs with different mass ratios $q \equiv m_2/m_1$ as a function of the binary total mass $M_{12} = m_1 + m_2$ for models with different particle numbers N (see Table 1) and different values for the mass

Table 1. Set of parameters of our model runs.

m_1 10^{-2}	m_2 10^{-2}	M_{12} 10^{-2}	q	μ 10^{-2}	025k	050k	100k	200k	400k	1M
(1)	(2)	(3)	(4)	(5)	(6)	(7)	(8)	(9)	(10)	(11)
1	0.01	1.01	0.010	0.0099	—	—	450	—	—	—
1	0.02	1.02	0.020	0.0196	—	—	450	—	—	—
1	0.03	1.03	0.030	0.0291	—	—	350	—	—	—
1	0.05	1.05	0.050	0.0476	—	—	350	—	—	—
1	0.10	1.10	0.100	0.0909	250	250	250*	250	250	150
1	0.20	1.20	0.200	0.1666	250	250	250*	250	250	150
1	0.50	1.50	0.500	0.3333	250	250	250*	250	250	150
1	1.00	2.00	1.000	0.5000	250	250	250*	250	250	150
2	0.02	2.02	0.010	0.0198	—	—	450	—	—	—
2	0.03	2.03	0.015	0.0295	—	—	450	—	—	—
2	0.05	2.05	0.025	0.0488	—	—	350	—	—	—
2	0.10	2.10	0.050	0.0952	—	—	350	—	—	—
2	0.20	2.20	0.100	0.1818	—	—	250	—	—	—
2	0.40	2.40	0.200	0.3333	—	—	250	—	—	—
2	1.00	3.00	0.500	0.6666	250	250	250	250	250	150
2	2.00	4.00	1.000	1.0000	250	250	250	250	250	150
4	0.04	4.04	0.010	0.0396	—	—	450	—	—	—
4	0.08	4.08	0.020	0.0784	—	—	450	—	—	—
4	0.10	4.10	0.025	0.0976	—	—	350	—	—	—
4	0.20	4.20	0.050	0.1905	—	—	350	—	—	—
4	0.40	4.40	0.100	0.3636	—	—	250	—	—	—
4	0.80	4.80	0.200	0.6666	—	—	250	—	—	—
4	2.00	6.00	0.500	1.3333	250	250	250	250	250	150
4	4.00	8.00	1.000	2.0000	250	250	250	250	250	150

Notes. Final integration time in *N*-body units. Col. 1 – 2: SMBH masses (primary and secondary, respectively) in a 10^{-2} model units. Col. 3: Total mass $M_{12} = m_1 + m_2$ in 10^{-2} model units. Col. 4: Mass ratio $q = m_2/m_1$, where $m_2 \geq m_1$. Col. 5: Reduced mass $\mu \equiv m_1 m_2/(m_1 + m_2)$ in 10^{-2} model units. Col. 6 – 11: Particle number in the stellar galactic nucleus. *: in these simulations, we performed two independent sets of runs. After the first set of runs, where the initial orbital velocity of the SMBH was exactly circular, V_{circ}, we ran a second set of runs where the initial velocity of the SMBHs was $V_{red} = 0.1\ V_{circ}$.

of the primary SMBH. The plot outlines how, at a fixed SMBHB total mass, a heavier primary – that is to say a lower mass ratio – determines larger hardening. Similarly, at a fixed primary mass, we see that heavier binaries – that is to say heavier companions – are associated with a smaller hardening rate. This implies that the efficiency of stellar hardening is maximized for low-mass-ratio SMBHBs with a heavy primary mass. This result holds regardless of the number of particles used, thus confirming that is a physical effect rather than a numerical one.

Taking advantage of scattering experiments, Rasskazov & Merritt (2017) and Rasskazov et al. (2019) recently showed that for low mass ratios ($q < 10^{-2}$), the hardening rate is proportional to $(1 + q)^2/q$. We find a similar dependence in our full *N*-body models, namely that the hardening is tightly linked to a simple combination of the binary primary mass and mass ratio defined as follows:

$$f(q,\mu) \equiv \frac{m_1 q}{(1 + q)^2} = \frac{m_2}{(1 + q)^2} = \frac{\mu}{(1 + q)}. \tag{1}$$

Figure 3 shows the relation between the hardening rate and the $\mu/(1 + q)$ quantity. We find that this relation is well fitted by the following simple exponential formula:

$$s_{fit} = \frac{d}{dt}\left(\frac{1}{a}\right) = A \exp\left(-\frac{B\mu}{1+q}\right), \tag{2}$$

with A=17.5 ± 0.3 and B=186.7 ± 8.8. We note that this relation implies that the secondary mass and the total mass ratio play the most effective role in shaping the SMBHB evolution. Also we fitted the data from Table 1 (Quinlan 1996) for systems with masses of m_1=0.01, 0.02, and 0.04 and obtained $B_{0.01}$=88.6, $B_{0.02}$=44.3, and $B_{0.04}$=22.1 accordingly when A=23.0 for all models.

The fitting formula provided above enables us to link the binary hardening rate to the masses of the binary components. Figure 3 compares our fitting formula with the simulated data for the 52 largest *N* models considered here. We see that in passing from $\mu/(1+q) = 10^{-4}$ to 10^{-2}, the hardening rate decreases by a factor of 5. At a fixed primary mass, this implies that highly asymmetric binaries ($q \ll 1$) tend to be characterized by a more effective hardening compared to the case of nearly equal mass SMBHBs. This might crucially affect the merger efficiency of SMBHBs in minor galaxy mergers, which are expected to be the main contributors to the population of SMBHBs with a mass ratio from

1:10-1:3, especially at high redshift (e.g. Callegari et al. 2011). Our results might have interesting consequences for GW astronomy since primary SMBHs with a mass from $10^6 - 10^7$ M$_\odot$ merging with a small companion might be bright GW sources for LISA (Amaro-Seoane et al. 2017) and similar space-based detectors such as TianQin (Luo et al. 2016), Taiji (Ruan et al. 2020), or μAres (Sesana et al. 2019).

3.2. Merger efficiency

We can use these results to place constraints on the SMBH merger efficiency. The long-term evolution of an SMBH binary can be written as follows (e.g. Gualandris & Merritt 2012; Arca-Sedda & Gualandris 2018; Gualandris et al. 2022):

$$\frac{da}{dt} = \frac{da}{dt}\Big|_* + \frac{da}{dt}\Big|_{GW}, \tag{3}$$

$$\frac{de}{dt} = \frac{de}{dt}\Big|_* + \frac{de}{dt}\Big|_{GW}, \tag{4}$$

where the asterisk identifies stellar hardening, whereas GW refers to the hardening driven by GW emission.

While the stellar hardening term in our simulations is a direct consequence of continuous star-SMBHB interactions and can be described through the adimensional hardening rate described in the previous section, the GW term for the evolution of semi-major axes is given by the following (Peters & Mathews 1963; Peters 1964a,b):

$$\frac{da}{dt}\Big|_{GW} = -\frac{64\beta}{5}\frac{F(e)}{a^3}, \tag{5}$$

$$\beta = \frac{G^3}{c^5 m_1 m_2 (m_1 + m_2)}, \tag{6}$$

$$F(e) = (1 - e^2)^{-7/2}\Big(1 + \frac{73}{24}e^2 + \frac{37}{96}e^4\Big). \tag{7}$$

The eccentricity evolution regulated by stellar encounters and GW emission, respectively, is given by the following:

$$\frac{de}{dt}\Big|_* = \frac{K}{a}\frac{da}{dt}, \tag{8}$$

$$\frac{de}{dt}\Big|_{GW} = -\frac{304\beta}{15}\frac{eD(e)}{a^4}, \tag{9}$$

$$D(e) = (1 - e^2)^{5/2}\Big(1 + \frac{121}{304}e^2\Big), \tag{10}$$

$$K = \frac{de}{d\ln(1/a)}, \tag{11}$$

where K is the eccentricity growth rate (Quinlan 1996). As shown in several recent works, the K parameter depends, nontrivially, on the MBH masses and the environment (see e.g. Wang et al. 2014; Bonetti et al. 2020). Due to this, in the following we neglect equation 8, thus implicitly assuming that the star-SMBHB interaction does not alter the binary eccentricity significantly (see e.g. Fig. 3 in Wang et al. 2014).

We solved the system of differential equations 5 – 11 numerically. We also adopted the scaling relation obtained for the adimensional hardening rate derived in equation 2, integrating the evolution of SMBH binaries down to the merger.

To obtain clues about the role played by our stellar hardening recipe on the formation of SMBH mergers, we created a sample of 2,000 SMBH binary mergers as follows. Firstly, we selected the primary and companion SMBH mass between $10^4 - 10^9$ M$_\odot$, adopting a uniform distribution in logarithmic
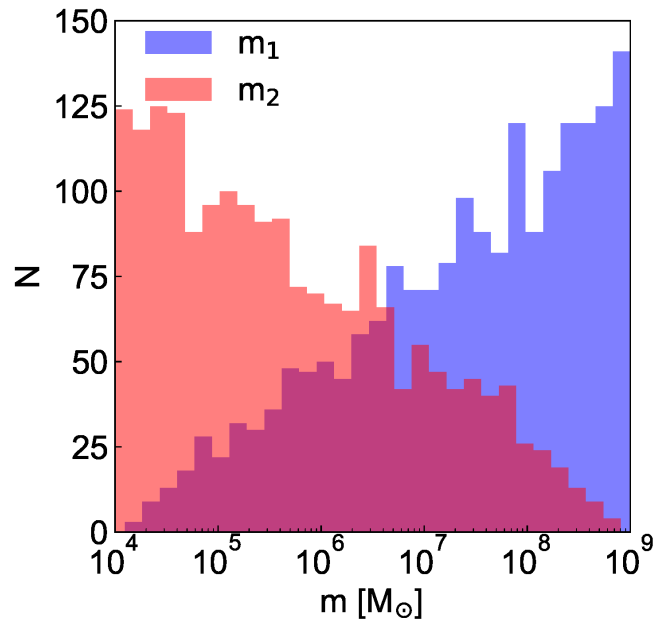

Fig. 4. Distribution of the random realization component masses $m_{1,2}$ ($m_2 \geq m_1$) for merging systems (subsection 3.2). The mass range in the middle (cherry colour) shows the overlapping masses.

values. We assumed that the SMBH host nucleus has a mass extracted from between $10^{1.5}$ and 10^4 times the SMBH mass (the values are in the range from the Milky Way to the classical bulges; Kormendy & Ho 2013), also adopting a uniform distribution in logarithmic values in this case.

In the Figure 4, we show the random realizations SMBH individual masses $m_{1,2}$. As we can see, our random sampling thoroughly cover the observed range of SMBHs. This implies nuclei with masses in the range $M_b = (3.5 \times 10^5 - 10^{13})$ M$_\odot$. For each pair, we calculated the hard-binary semi-major axis $a_h = G(m_1 + m_2)/2\sigma^2$, evaluating the galaxy velocity dispersion from the $M_{SMBH} - \sigma$ relation (Gültekin et al. 2009; Kormendy & Ho 2013). We started our integration assuming that the binary semi-major axis equals the hard-binary separation and we drew the eccentricity from a thermal distribution[3] (Jeans 1919; Ambartsumian 1937; Heggie 1975; Kroupa 2008).

In Figure 5, we show T_{merge} as a function of the $\mu/[M_b(1+q)]$ parameter (varying the binary mass ratio and primary mass) and the individual masses of the SMBHB. Looking at the two panels in the figure highlights the role of stellar hardening in the SMBHB evolution, leading the actual merger time to the range of $\sim 10^7$ yr, which is many orders of magnitude larger as a simple merger timescale estimation based on the Peters-Mathews formalism (Peters & Mathews 1963; Peters 1964a,b). At a fixed SMBH primary mass, our results show that the minimization of the merger time is achieved for binaries with lighter SMBH companions, thus with lower mass ratios. This is due to the fact that lower mass ratios imply lower values for the $\mu/[M_b(1 + q)]$ parameter, which in turn implies a larger hardening in terms of absolute values. The efficient hardening driven by the rotating nucleus thus enables SMBHBs with mass ratios of $q = 10^{-4} - 1$ and component masses of $m_{1,2} = 10^{4-9}$ M$_\odot$ (Fig. 4) to merge over timescales, that is $T_{merge} \approx 10^3 - 10^7$ yr.

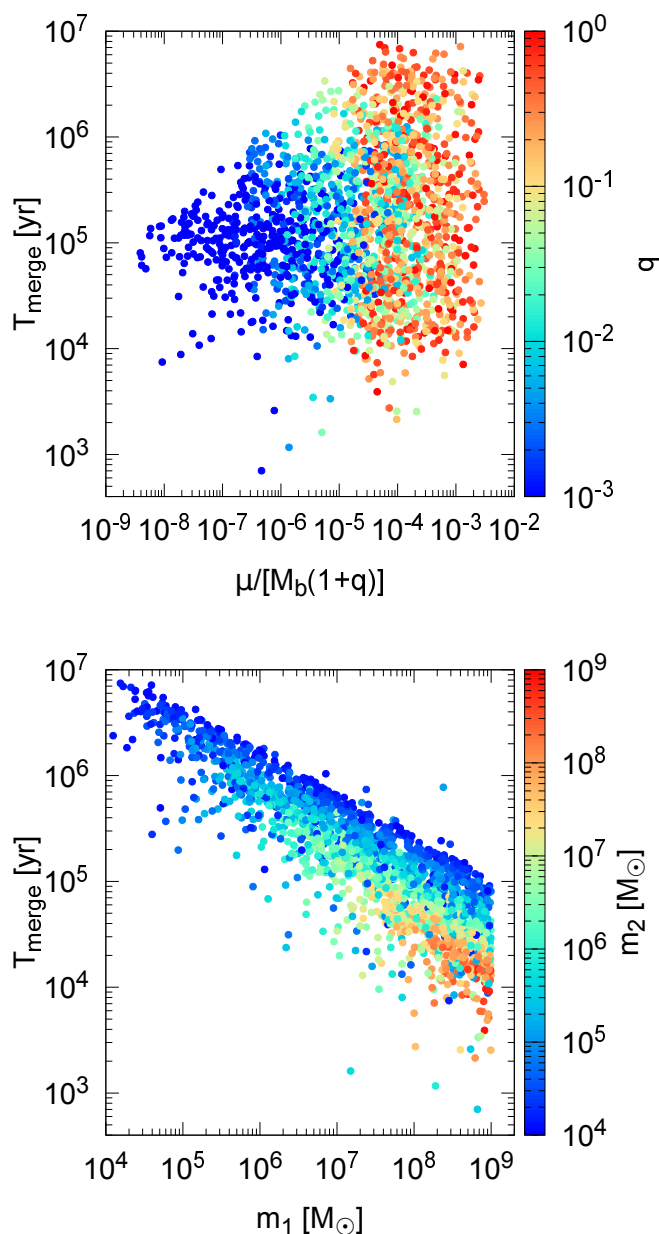[3] We also tried to use a uniform distribution and found no significant differences in the results.

Fig. 5. *Top panel:* Merger time T_{merge} as a function of the $\mu/[M_b(1 + q)]$ parameter conveniently scaled to the galaxy nucleus mass M_b. The colour coding identifies the binary mass ratio. *Bottom panel:* Merger time T_{merge} as a function of the primary mass m_1, where colour coding identifies the secondary mass m_2.

4. Summary

We have presented a systematic study of the evolution of asymmetric SMBH binaries harboured in a non-axisymmetric, dense stellar galactic nucleus. To be able to perform this large systematic set of direct *N*-body simulations, we have developed a new high-performance computing code φ−GPU that enables one to fully exploit current and next generations high-performance GPU clusters.

Our simulations suggest that the binary hardening rate for unequal mass SMBHBs does not depend on the number of particles *N*, at least in the regime investigated here. The stellar hardening in our modelled SMBHBs is sufficiently effective to drive

the SMBHB towards coalescence in a short timescale of about a gigayear (Berentzen et al. 2009).

For a fixed mass of the primary SMBH, that is the more massive one, we find a significant increase in the hardening rate for smaller masses of the secondary (i.e. lighter) SMBH. On the other hand, for a fixed mass of the secondary SMBH, we find the hardening rate to be proportional to the primary's mass.

We find a tight relation between the hardening rate and the binary total mass M_{12} and reduced mass μ, which suggests that the SMBHB shrinkage process can be described by a two-parameters' relation. Smaller values of M_{12} and μ result in an increase in the hardening rate. The hardening rates in our models support predictions of three-body scatter experiments (see e.g. Hills & Fullerton 1980; Hills 1983; Rasskazov & Merritt 2017; Rasskazov et al. 2019), which suggests a scaling between the hardening rate and binary mass ratio.

References

Aarseth S. J., Henon M., Wielen R., 1974, A&A, 37, 183
Amaro-Seoane P., et al., 2013, GW Notes, 6, 4
Amaro-Seoane P., et al., 2017, arXiv e-prints, p. arXiv:1702.00786
Ambartsumian V. A., 1937, AZh, 14, 207
Arca-Sedda M., Gualandris A., 2018, MNRAS, 477, 4423
Bansal K., Taylor G. B., Peck A. B., Zavala R. T., Romani R. W., 2017, ApJ, 843, 14
Begelman M. C., Blandford R. D., Rees M. J., 1980, Nature, 287, 307
Berczik P., Merritt D., Spurzem R., Bischof H.-P., 2006, ApJ, 642, L21
Berczik P., et al., 2011, in International conference on High Performance Computing, HPC-UA 2011. pp 8–18
Berczik P., Spurzem R., Wang L., 2013a, in Third International Conference on High Performance Computing, HPC-UA 2013. pp 52–59 (arXiv:1312.1789)
Berczik P., Spurzem R., Zhong S., Wang L., Nitadori K., Hamada T., Veles A., 2013b, in Kunkel J. M., Ludwig T., Meuer H., eds, Lecture Notes in Computer Science Vol. 7905, Procs. of 28th Intl. Supercomputing Conf. ISC 2013, Leipzig, Germany, June 16-20, 2013. Springer, Berlin, Heidelberg, pp 13–25, doi:https://doi.org/10.1007/978-3-642-38750-0_2
Berentzen I., Preto M., Berczik P., Merritt D., Spurzem R., 2009, ApJ, 695, 455
Bonetti M., et al., 2020, MNRAS, 493, L114
Callegari S., Kazantzidis S., Mayer L., Colpi M., Bellovary J. M., Quinn T., Wadsley J., 2011, ApJ, 729, 85

Einsel C., Spurzem R., 1999, MNRAS, 302, 81
Fabbiano G., Paggi A., Karovska M., Elvis M., Nardini E., Wang J., 2020, ApJ, 902, 49
Gong X., et al., 2011, Classical and Quantum Gravity, 28, 094012
Gualandris A., Merritt D., 2012, ApJ, 744, 74
Gualandris A., Khan F. M., Bortolas E., Bonetti M., Sesana A., Berczik P., Holley-Bockelmann K., 2022, MNRAS, 511, 4753
Gültekin K., et al., 2009, ApJ, 698, 198
Harfst S., Gualandris A., Merritt D., Spurzem R., Portegies Zwart S., Berczik P., 2007, New A, 12, 357
Heggie D. C., 1975, MNRAS, 173, 729
Hills J. G., 1983, AJ, 88, 1269
Hills J. G., Fullerton L. W., 1980, AJ, 85, 1281
Ho L. C., Kim M., 2014, ApJ, 789, 17
Iwasawa M., An S., Matsubayashi T., Funato Y., Makino J., 2011, ApJ, 731, L9
Jeans J. H., 1919, MNRAS, 79, 408
Jülich Supercomputing Centre 2021, Journal of large-scale research facilities, 7
Just A., Yurin D., Makukov M., Berczik P., Omarov C., Spurzem R., Vilkoviskij E. Y., 2012, ApJ, 758, 51
Khan F. M., Holley-Bockelmann K., Berczik P., Just A., 2013, ApJ, 773, 100
Khan F. M., Fiacconi D., Mayer L., Berczik P., Just A., 2016, ApJ, 828, 73
Khan F. M., Capelo P. R., Mayer L., Berczik P., 2018, ApJ, 868, 97
Kollatschny W., Weilbacher P. M., Ochmann M. W., Chelouche D., Monreal-Ibero A., Bacon R., Contini T., 2020, A&A, 633, A79
Komossa S., Burwitz V., Hasinger G., Predehl P., Kaastra J. S., Ikebe Y., 2003, ApJ, 582, L15
Kormendy J., Ho L. C., 2013, ARA&A, 51, 511
Kroupa P., 2008, in Aarseth S. J., Tout C. A., Mardling R. A., eds, The Cambridge N-Body Lectures Vol. 760, Lecture Notes in Physics. Springer-Verlag Berlin Heidelberg, pp 181–259, doi:10.1007/978-1-4020-8431-7_8
Li S., Liu F. K., Berczik P., Chen X., Spurzem R., 2012, ApJ, 748, 65
Luo J., et al., 2016, Classical and Quantum Gravity, 33, 035010
Makino J., Funato Y., 2004, ApJ, 602, 93
Mikkola S., Valtonen M. J., 1992, MNRAS, 259, 115
Naab T., Jesseit R., Burkert A., 2006, MNRAS, 372, 839
Naab T., Johansson P. H., Ostriker J. P., 2009, ApJ, 699, L178
Nitadori K., Makino J., 2008, New A, 13, 498
Peters P. C., 1964a, PhD thesis, California Institute of Technology
Peters P. C., 1964b, Physical Review, 136, 1224
Peters P. C., Mathews J., 1963, Physical Review, 131, 435
Quinlan G. D., 1996, New A, 1, 35
Rasskazov A., Merritt D., 2017, ApJ, 837, 135
Rasskazov A., Fragione G., Leigh N. W. C., Tagawa H., Sesana A., Price-Whelan A., Rossi E. M., 2019, ApJ, 878, 17
Rodriguez C., Taylor G. B., Zavala R. T., Peck A. B., Pollack L. K., Romani R. W., 2006, ApJ, 646, 49
Ruan W.-H., Guo Z.-K., Cai R.-G., Zhang Y.-Z., 2020, International Journal of Modern Physics A, 35, 2050075
Sesana A., et al., 2019, arXiv e-prints, p. arXiv:1908.11391
Sobolenko M., Berczik P., Spurzem R., Kupi G., 2017, Kinematics and Physics of Celestial Bodies, 33, 21
Sobolenko M., Berczik P., Spurzem R., 2021, A&A, 652, A134
Valtonen M. J., 2007, ApJ, 659, 1074
Valtonen M. J., et al., 2010a, Celestial Mechanics and Dynamical Astronomy, 106, 235
Valtonen M. J., et al., 2010b, ApJ, 709, 725
Voggel K. T., et al., 2022, A&A, 658, A152
Wang L., Berczik P., Spurzem R., Kouwenhoven M. B. N., 2014, ApJ, 780, 164
Zhong S., Berczik P., Spurzem R., 2014, ApJ, 792, 137